

On the linear analysis of unstable radiative shocks

Babulakshmanan Ramachandran^{*} & Michael D. Smith[†]

Armagh Observatory, College Hill, Armagh BT61 9DG, Northern Ireland

Accepted Received ; in original form

ABSTRACT

We study the stability properties of strong hydrodynamic shocks and their associated radiative cooling layers. We explore a range of conditions which covers both molecular and atomic gas impacting against a rigid wall. Through a linear analysis employing a cooling function of the form $\Lambda \propto \rho^\beta T^\alpha$ and a specific heat ratio of γ , we determine the overstability regime in the parameter space consisting of α , β and γ . In general, if α is sufficiently low, the fundamental mode leads to long wavelength growing oscillations. For the fundamental mode, we find that values of γ corresponding to molecular hydrodynamics lead to a significantly restricted instability range for α in comparison to the shocks in a monatomic medium. The conditions for the growth of higher order modes, however, are relatively unchanged. This predicts that certain molecular shocks are prone to display signatures of small-scale rapid variability. Dissociative shocks, however, can be subject to a large-scale overstability if subsequent molecule formation in the cooling layer abruptly increases the cooling rate. In contrast to the dynamical rippling overstability, the cooling overstability is suppressed for a sufficiently low specific heat ratio.

Key words: hydrodynamics – instabilities – shock waves – ISM: – ISM: molecules

1 INTRODUCTION

Under many astrophysical conditions, heated gas cools rapidly after the passage of a shock front. Radiative shocks are defined as those shock waves in which the time scale for cooling is much shorter than the appropriate dynamical or evolutionary time scale of the system that drives the shock (McKee & Hollenbach 1980; Draine & McKee 1993). They stand as cornerstones which help us recognise and interpret a wide variety of astrophysical phenomena such as encountered in the columns of matter accreting onto degenerate stars, Herbig-Haro objects associated with young stars, the remnants of old supernova and planetary nebula. Indeed, predictions for radiative shocks have been employed to confirm a great deal of our understanding of astrophysical flows (e.g. Fischer & Beuermann 2001; Hartigan et al. 1987; Hollenbach & McKee 1989; Fesen et al. 1992). However, many predictions are based on the often crude assumption that the shock wave is steady and much work has been expended to justify this (see below). With the regular treatment of new types of radiative shocks, such as within molecular clouds, new analyses become necessary. Here, we undertake a general linear stability analysis in order to cover a diverse range of shock types, with the main intention of extending previ-

ous studies by exploring the stability conditions of shocks which pass through molecular media.

While modelling the accretion of matter onto stellar surfaces, Langer et al. (1981) discovered that the stand-off radiative shocks exhibit oscillations due to the onset of thermal instability. They gave results for the case of bremsstrahlung cooling for which the cooling rate per unit volume is $\Lambda \propto \rho^2 T^{1/2}$ where ρ is the density and T is the temperature. Their computations showed that the shock structure is unstable when bremsstrahlung dominates.

Soon after, Chevalier & Imamura (1982, hereafter CI82) performed a linear stability analysis for plane parallel flows with $\Lambda \propto \rho^2 T^\alpha$. They found that such shocks were linearly unstable in a fundamental mode if the exponent $\alpha \lesssim 0.4$ and unstable to overtones for $\alpha \lesssim 0.8$. The physical basis for the instability is that, while the shock wave is moving away from the surface, it heats the gas to a higher temperature and the cooling time is longer than in the steady state case. As a result, in the unstable regime, the shock structure attempts to form an even larger cooling region. In contrast, while the shock wave is moving in, the situation is reversed thus yielding amplified oscillations i.e. overstability.

The linear analysis was subsequently confirmed by numerical simulations (Imamura et al. 1984). Bertschinger (1986) extended the linear analysis to three dimensions and showed that modes with transverse velocities would be unstable for $\alpha \lesssim 1.0$. Observationally optical quasi-periodic oscillations are seen in several strong field (polar) cataclysmic

^{*} E-mail: brc@arm.ac.uk

[†] E-mail: mds@arm.ac.uk

variables while only upper limits have been obtained for the corresponding X-ray variability (Larsson 1992; Wolff et al. 1999).

A range of numerical and linear analyses have catered for hot atomic gases in various physical and geometric guises (Dgani & Soker 1994; Imamura et al. 1996; Strickland & Blondin 1995; Sutherland et al. 2003). Until now there has never been an analytical formulation specifically for the molecular case. Cooling functions of the form $\Lambda \propto \rho T^\alpha$ were studied by Imamura (1985) and Saxton et al. (1998) with cyclotron and Compton cooling in mind. Houck & Chevalier (1992) examined a case with a specific heat ratio of $\gamma = 4/3$ under spherical geometry, with neutrino cooling in a gas dominated by radiation pressure (for which $\alpha = \beta = 5/2$). Imamura et al. (1996, see their Appendix B) presented a linear analysis which covered a cooling function of the form

$$\Lambda \propto \rho^\beta T^\alpha \quad (1)$$

but maintained $\gamma = 5/3$. This clearly demonstrated that the instability criterion depends more on $\beta - \alpha$ than on α or β separately and, therefore, that lowering β tends to restrict the instability regime.

There have been recent suggestions that shocks into a molecular medium may be unstable. Numerical simulations in one dimension found the instability to be present when the shock is sufficiently fast to dissociate the molecules (Smith & Rosen 2003, hereafter SR03). Then, accelerated cooling within the cooling layer brings about the overstability. To occur, it was found that either carbon or oxygen has to be present and the gas sufficiently dense so that reforming water and carbon monoxide molecules provide the accelerated cooling in the compressed gas. Although clearly linked to the overstability discussed here, it was noted that an improved non-equilibrium treatment of the chemistry would mollify the overstability. Recently, a high resolution study by Lesaffre et al. (2004) has revealed that large amplitude oscillations arise only just above the dissociation speed limit ($25 - 30 \text{ km s}^{-1}$) while short-period low-amplitude oscillations occur at higher speeds.

Here, we clarify the regime of shock stability by exploring the entire $[\alpha, \beta, \gamma]$ parameter space. By generalising the density index, we take into account different physical situations. In particular, $\beta = 1$ corresponds to cases where the energy levels of the atoms or molecules which provide the dominant cooling are in local thermodynamic equilibrium. For example, this can be H_2 cooling in warm gas for densities above $\sim 10^4 \text{ cm}^{-3}$ provided hydrogen atoms act as the main collision partner. The specific heat ratio $\gamma = 5/3$ remains appropriate for dissociative shocks. The value $\gamma = 7/5$ applies to a pure H_2 gas while, more realistically for the interstellar medium, $\gamma = 10/7$ accounts for the addition of ten per cent helium atoms.

We also consider the case $\gamma = 21/19$. This may approximately simulate a shock with two cooling components, one of which operates in an extremely thin layer immediately following the shock front. This effectively provides a strong shock compression, providing a rigidity which we suspect will stabilise a shock. Physically, this corresponds to rapid atomic cooling which follows dissociative shocks, bringing the temperature back down to about 8000 K. The subsequent molecular, dust or atomic fine-structure cooling then occurs over an extended zone to which the linear stability

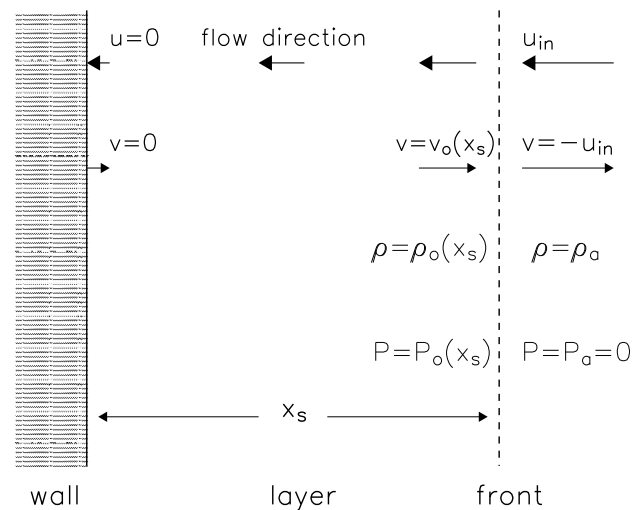


Figure 1. A sketch of the steady shock configuration. The shock jump conditions are defined by Eqs 5, 6 and 7. Note that under strong shock conditions, the upstream pressure is equated to zero.

analysis applies. This case, however, is here presented to exemplify the consequences of making the assumption of near-isothermality in numerical simulations. This assumption is sometimes applied in order to avoid resolving the cooling layer. However, it is important to qualify if the conditions would produce the correct physical behaviour.

In this first study, we ignore the magnetic field and also we restrict ourselves to one dimension. We start by calculating the steady state radiative shock structure. We then introduce small perturbations to the shock velocity and try to determine both growth as well as damping rates in addition to the oscillatory period in the parameter space. Note that thermal conduction and radiation transfer are also ignored.

To determine the overall effect, it is necessary to consider the stability of the full configuration, of which the radiative shock is only one component. Firstly, sufficient time must pass for a steady state to be reached. Secondly, there are numerous instabilities which may be even more effective. These tend to disrupt the accumulating gas layer either between two shocks or between a single shock and a medium of high thermal pressure. The instabilities include the Vishniac thin-shell linear instability (Vishniac 1983; Mac Low & Norman 1993) the non-linear thin shell instability (Vishniac 1994) and the transverse acceleration instability (Dgani et al. 1996). The conditions for gravitational instability within the radiative cooling layer itself is also of relevance in the cosmological context (Birnbom & Dekel 2003).

2 METHOD

2.1 The steady state solution

Following CI82, we consider matter of constant density ρ_a and speed u_{in} which is incident on a stationary wall, as sketched in Fig. 1. The approach speed u_{in} is defined as a positive quantity. Therefore, the pre-shock gas velocity is

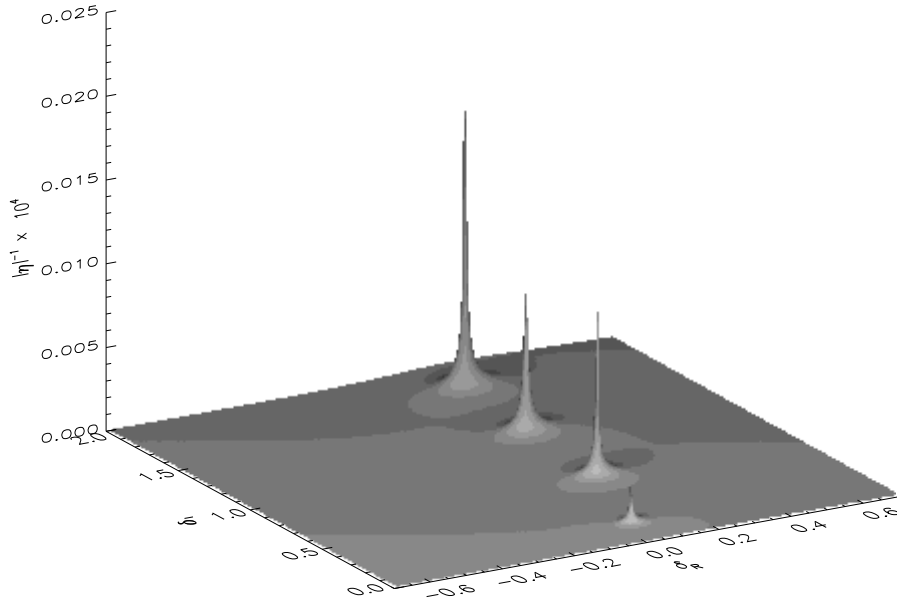


Figure 2. Graphical representation of the various modes for the case $\alpha = -1$, $\beta = 2$ and $\gamma = 7/5$. The spikes in the figure correspond to the normalised eigenfrequencies where $\delta = (x_{s0}/u_{in}) \sigma$ and σ is the eigenfrequency.

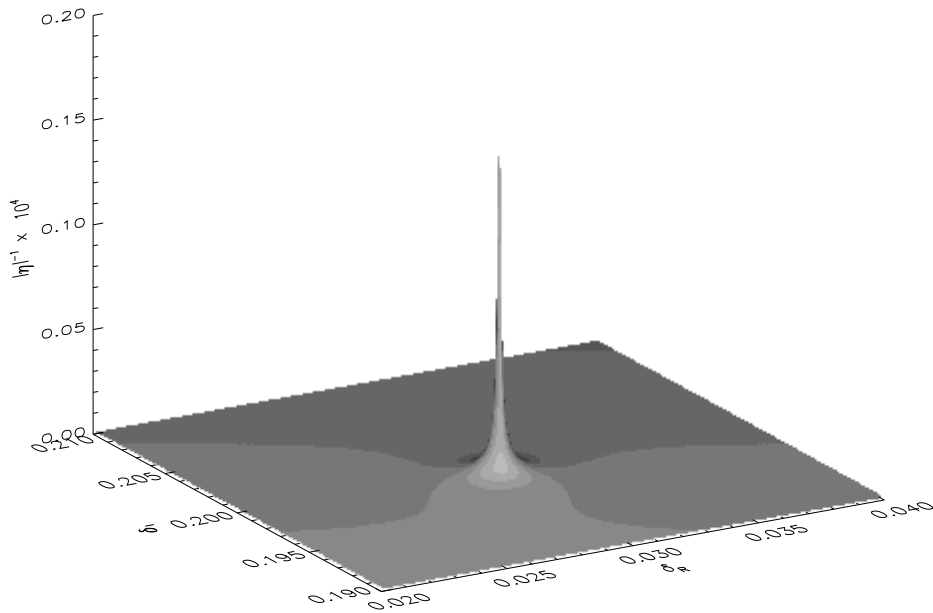


Figure 3. High-resolution graphical representation of a single mode corresponding to the case $\alpha = -1$, $\beta = 2$ and $\gamma = 7/5$. The spike corresponds to the eigenfrequency of the fundamental mode.

$v = -u_{in}$. In this one dimensional setup, the origin $x = 0$ is at the wall with the shock front being at some $x = x_s$. The post-shocked gas passes through the cooling region and is added to an infinitely thin region at the wall. The length x_s is the thickness of the cooling region. The one dimensional

hydrodynamical equations are

$$\frac{\partial \rho}{\partial t} + \rho \frac{\partial v}{\partial x} + v \frac{\partial \rho}{\partial x} = 0 \quad (2)$$

$$\rho \left(\frac{\partial v}{\partial t} + v \frac{\partial v}{\partial x} \right) + \frac{\partial P}{\partial x} = 0 \quad (3)$$

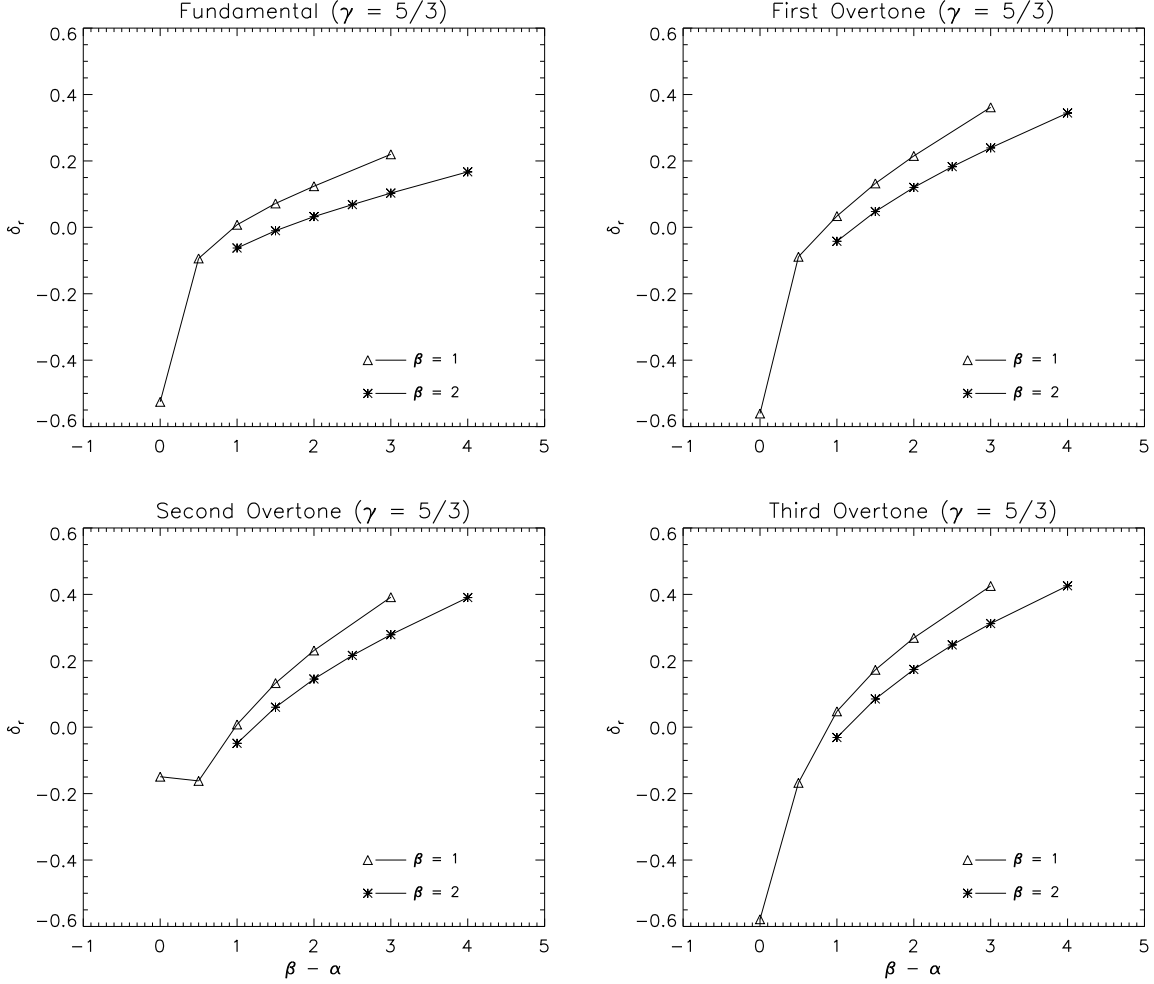


Figure 4. The linear growth rate δ_r is plotted versus $\beta - \alpha$ for $\gamma = 5/3$ for various modes. Here, the normalisation $\delta_r = (x_{s0}/u_{in})\sigma_r$ has been applied where σ_r is the real part of the frequency in absolute units.

$$\frac{\partial P}{\partial t} + v \frac{\partial P}{\partial x} - \frac{\gamma P}{\rho} \left(\frac{\partial \rho}{\partial t} + v \frac{\partial \rho}{\partial x} \right) = -(\gamma - 1)A\rho^{\beta-\alpha}P^\alpha \quad (4)$$

where equations (2), (3) & (4) refer to the conservation of mass, momentum and energy respectively. In equation (4), A is a constant and γ is the specific heat ratio. The steady state solution is denoted by the subscript 0. The Rankine-Hugoniot conditions give the values of the physical variables at $x = x_s$ which are (for a high Mach number):

$$\rho_0(x_s) = \left(\frac{\gamma + 1}{\gamma - 1} \right) \rho_a \quad (5)$$

$$v_0(x_s) = - \left(\frac{\gamma - 1}{\gamma + 1} \right) u_{in} \quad (6)$$

$$P_0(x_s) = \left(\frac{2}{\gamma + 1} \right) \rho_a u_{in}^2 \quad (7)$$

Equations (5), (6) & (7) are obtained when equations (2) and (3) are integrated to yield

$$\rho_0 v_0 = -\rho_a u_{in} \quad (8)$$

$$P_0 = \rho_a u_{in} (v_0 + u_{in}) \quad (9)$$

Equations (8) & (9) are substituted in equation (4) to get

$$\frac{dv_0}{dx} = \frac{(\gamma - 1)A(-\rho_a u_{in})^{\beta-1}}{v_0^\beta [v_0 + \gamma(v_0 + u_{in})] [-v_0^2 - u_{in}v_0]^{-\alpha}} \quad (10)$$

Hence, it is expedient to take the velocity as the independent variable in the ensuing analysis. Note that, as seen by taking the asymptotic limit $v_0 \rightarrow 0$ in equation (10) and integrating, the total shock length is finite only for $\alpha < 1 + \beta$. We now introduce the following variables

$$\xi = \frac{x}{x_s} \quad (11)$$

$$w = \frac{v_0}{u_{in}} \quad (12)$$

Equations (10), (11) and (12) lead to

$$\frac{d\xi}{dw} = \frac{-(-w)^\beta u_{in}^{3-2\alpha} [w + \gamma(1+w)] [-w(1+w)]^{-\alpha}}{(\gamma - 1)A\rho_a^{\beta-1} x_s} \quad (13)$$

We have to integrate eq. (13) with the boundary conditions

$$w = 0 \quad \text{at } \xi = 0, \quad (14)$$

$$w = - \left(\frac{\gamma - 1}{\gamma + 1} \right) \quad \text{at } \xi = 1. \quad (15)$$

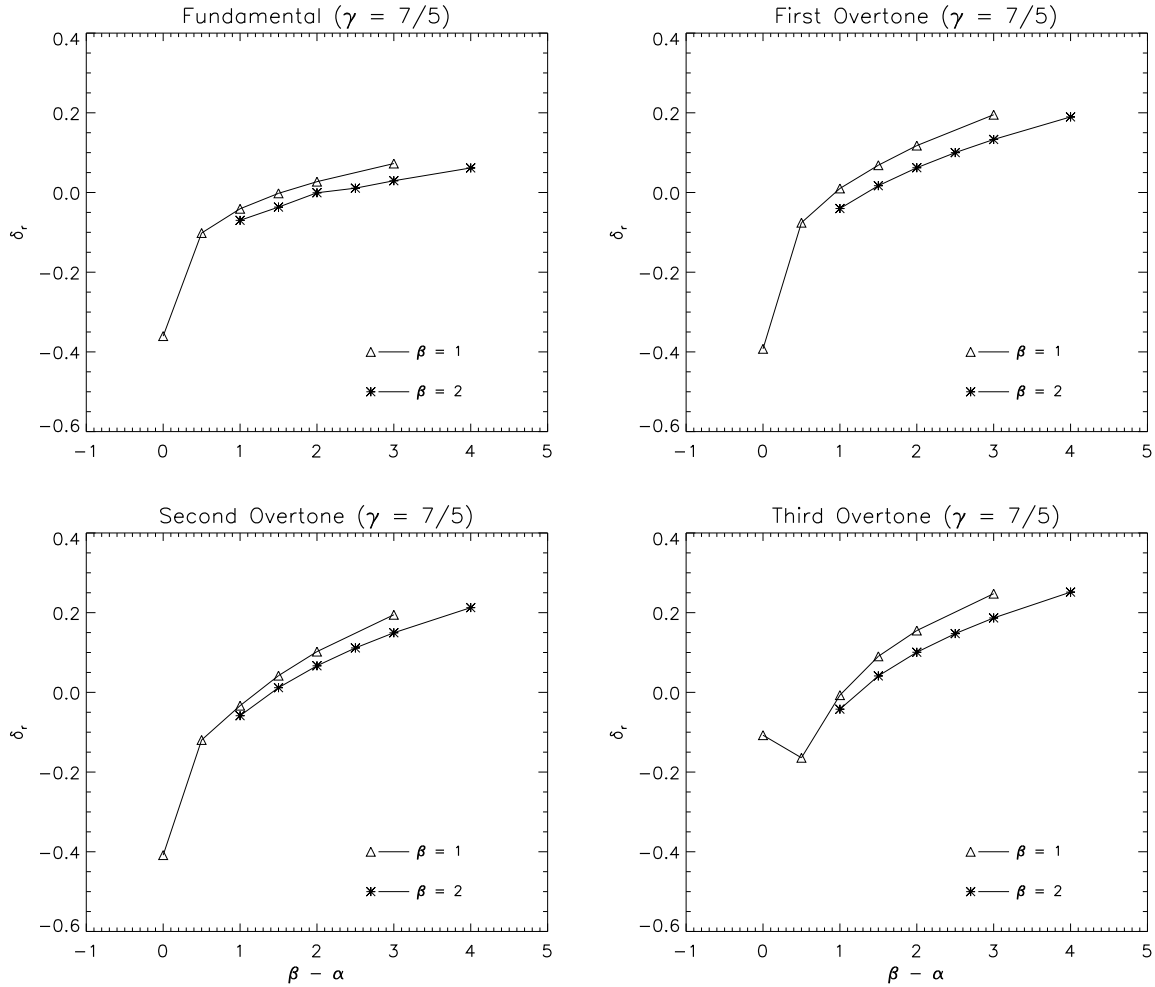


Figure 5. The linear growth rate δ_r is plotted versus $\beta - \alpha$ for $\gamma = 7/5$ for various modes. Here, the normalisation $\delta_r = (x_{s0}/u_{in}) \sigma_r$ has been applied where σ_r is the real part of the frequency in absolute units.

The shock width x_s is evaluated in the process. We have derived the analytical expressions for ξ for various cases (see Appendix B).

2.2 The set of linear equations

The shock wave is now perturbed by

$$\frac{dx_s}{dt} = v_{s1} e^{\sigma t} \quad (16)$$

where, $\sigma = \sigma_R + i\sigma_I$ is the frequency and v_{s1} is a real quantity. The position of the shock may be represented as the real part of

$$x_s = x_{s0} + x_{s1} e^{\sigma t} \quad (17)$$

where $x_{s1} = \frac{v_{s1}}{\sigma}$. Considering only the terms up to first

order:

$$\xi = \frac{x}{x_s} = \frac{x}{x_{s0}} \left(1 - \frac{x_{s1}}{x_{s0}} e^{\sigma t} \right) \quad (18)$$

$$\frac{\partial \xi}{\partial x} = \frac{1}{x_{s0}} \left(1 - \frac{x_{s1}}{x_{s0}} e^{\sigma t} \right) \quad (19)$$

$$\frac{\partial \xi}{\partial t} = -\frac{xx_{s1}\sigma e^{\sigma t}}{x_{s0}^2} \quad (20)$$

$$\rho = \rho_0(\xi) + \rho_1(\xi) e^{\sigma t} \quad (21)$$

$$P = P_0(\xi) + P_1(\xi) e^{\sigma t} \quad (22)$$

$$v = v_0(\xi) + v_1(\xi) e^{\sigma t}. \quad (23)$$

All the quantities with subscript 1 represent the small perturbed factors. The boundary conditions at the shock wave are (see Appendix A)

$$\rho_1 = 0 \quad (24)$$

$$P_1 = \left(\frac{4u_{in} v_{s1} \rho_a}{\gamma + 1} \right) \quad (25)$$

$$v_1 = \left(\frac{2v_{s1}}{\gamma + 1} \right) \quad (26)$$

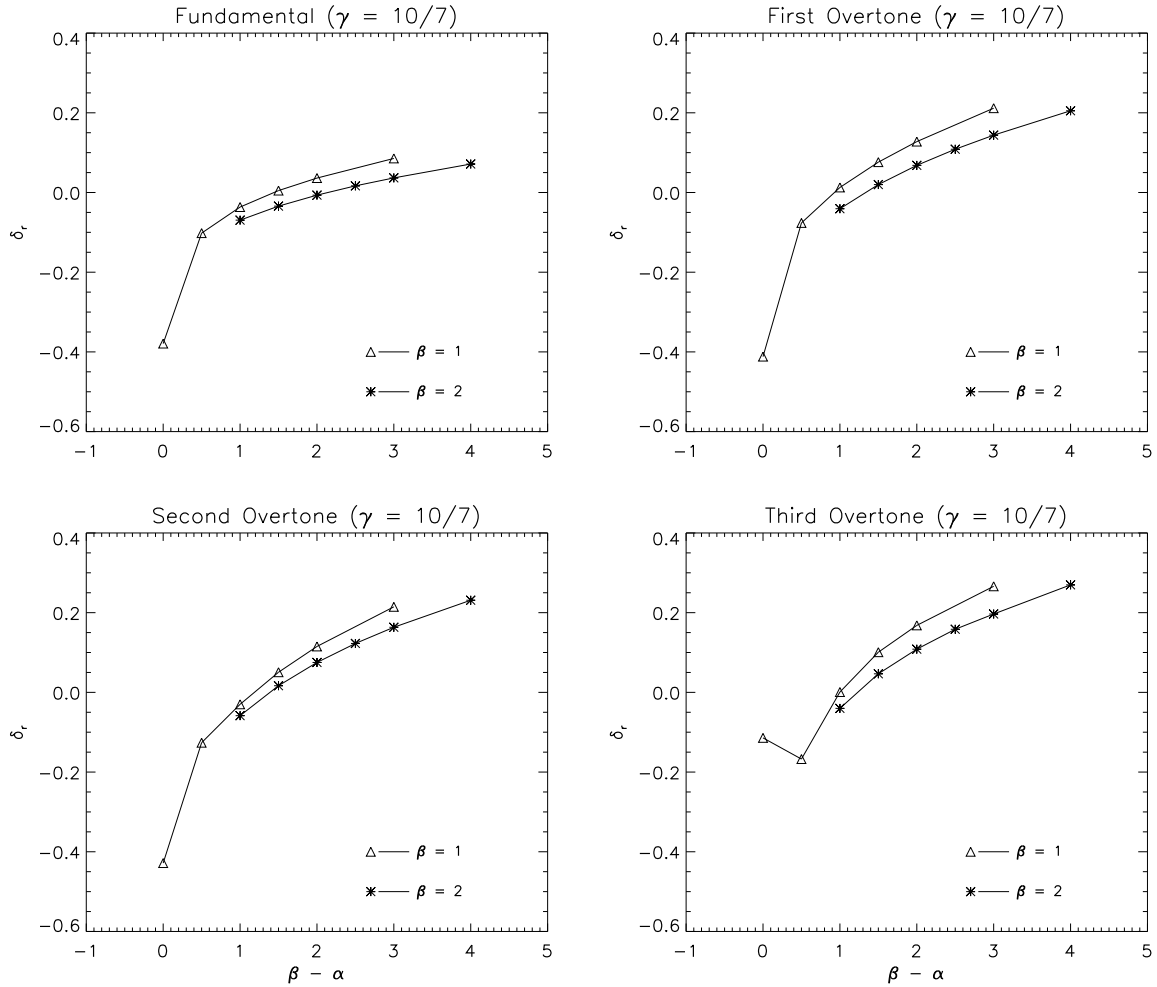


Figure 6. The linear growth rate δ_r is plotted versus $\beta - \alpha$ for $\gamma = 10/7$ for various modes. Here, the normalisation $\delta_r = (x_{s0}/u_{in}) \sigma_r$ has been applied where σ_r is the real part of the frequency in absolute units.

We then transform the following variables as

$$\zeta = \frac{x_{s0}\sigma\rho_1}{v_{s1}\rho_a} \quad (27)$$

$$\pi = \frac{P_1}{v_{s1}\rho_a u_{in}} \quad (28)$$

$$\eta = \frac{v_1}{v_{s1}} \quad (29)$$

$$\delta = \frac{x_{s0}\sigma}{u_{in}}. \quad (30)$$

Substituting (21), (22), (23) into (2), (3) and (4), the fluid equations become

$$-\frac{\xi}{w^2} + \zeta \frac{d\xi}{dw} + \frac{w}{\delta} \frac{d\zeta}{dw} + \frac{\eta}{w^2} - \frac{1}{w} \frac{d\eta}{dw} + \frac{\zeta}{\delta} = 0 \quad (31)$$

$$-\xi + \delta \frac{d\xi}{dw} \eta + w \frac{d\eta}{dw} + \eta - \frac{w^2}{\delta} \zeta - w \frac{d\pi}{dw} = 0 \quad (32)$$

$$D + E = F \quad (33)$$

where

$$D = \left[-\xi + \delta \frac{d\xi}{dw} \pi + w \frac{d\pi}{dw} + \eta - \frac{w}{\delta} + \pi \gamma \right]$$

$$E = \left(-\frac{\xi}{w^2} + \zeta \frac{d\xi}{dw} + \frac{w}{\delta} \frac{d\zeta}{dw} + \frac{\eta}{w^2} - \frac{1}{\delta w} + \frac{\zeta}{\delta} \right) \times (\gamma w(w+1))$$

$$F = [w + \gamma(1+w)] \times \left[\frac{\alpha\pi}{(1+w)} - (\beta - \alpha) \frac{w\zeta}{\delta} \right]$$

The quantities ζ , π and η are complex eigenfunctions where the subscript r denotes the real component and i stands for the imaginary part for each of the above quantities. The quantity δ is a complex number with the sign of the real part, δ_r , indicating the instability (+ve value) or stability (-ve value) of a mode. The quantity δ_i is interpreted as the eigenfrequency (in units of (u_{in}/x_{s0})).

From Eqs. (28), (29) and (30), we get six coupled first order equations which are

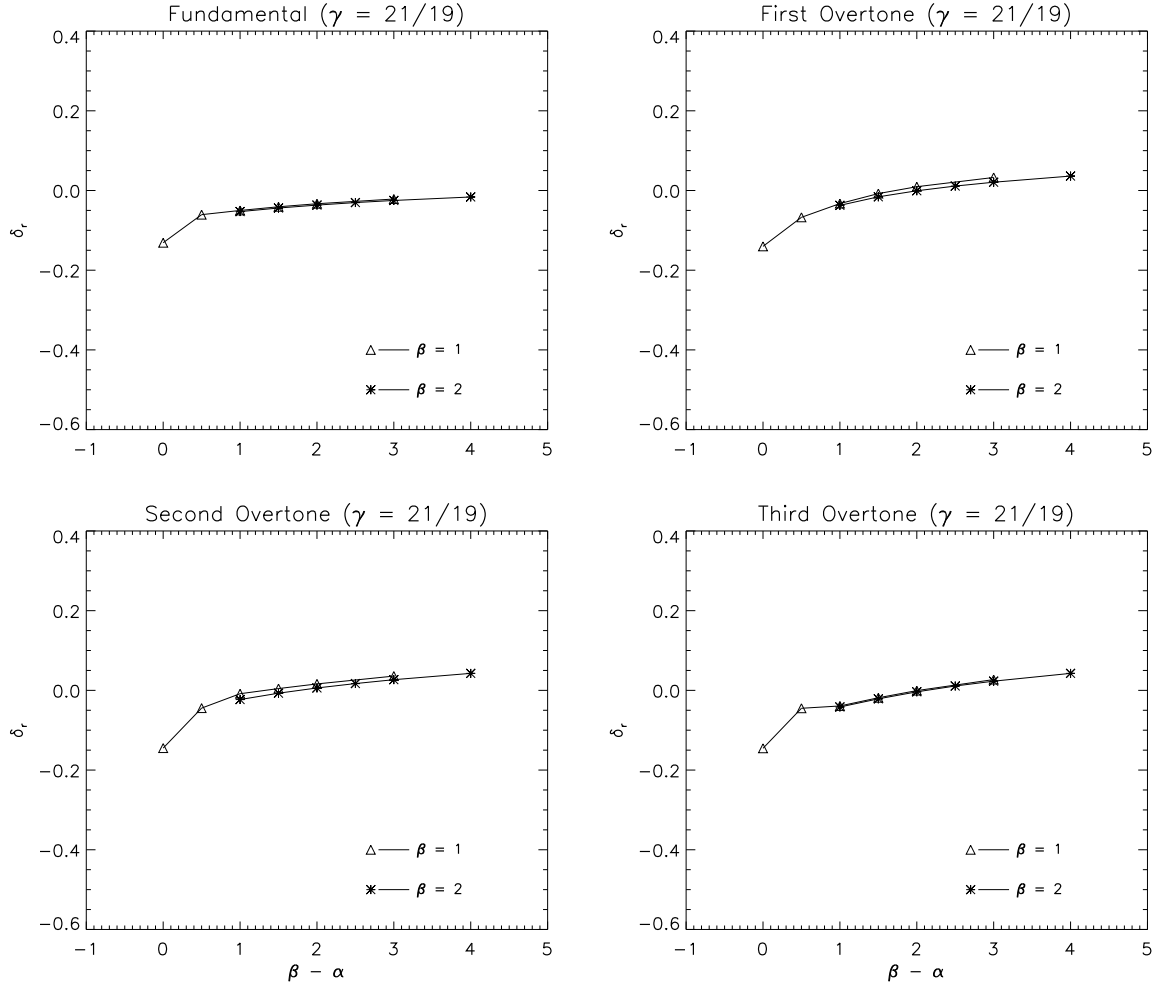


Figure 7. The linear growth rate δ_r is plotted versus $\beta - \alpha$ for $\gamma = 21/19$ for various modes. Here, the normalisation $\delta_r = (x_{s0}/u_{in}) \sigma_r$ has been applied where σ_r is the real part of the frequency in absolute units.

$$\frac{d\eta_r}{dw} = \frac{\alpha\pi_r}{w+1} - \frac{w(\beta-\alpha)(\delta_r\zeta_r + \delta_i\zeta_i)}{\delta^2} + \frac{\delta_r}{\delta^2} + \frac{2\xi\delta^2 - 2\eta_r\delta^2 - \gamma\pi_r\delta^2 + w^2(\zeta_r\delta_r + \zeta_i\delta_i)}{(w+\gamma(w+1))\delta^2} - \frac{d\xi}{dw} \left[\frac{\delta_r(\eta_r + \pi_r) - \delta_i(\eta_i + \pi_i)}{(w+\gamma(w+1))} \right] \quad (34)$$

$$\frac{d\eta_i}{dw} = \frac{\alpha\pi_i}{w+1} - \frac{w(\beta-\alpha)(\delta_r\zeta_i - \delta_i\zeta_r)}{\delta^2} - \frac{\delta_i}{\delta^2} + \frac{-2\eta_i\delta^2 - \gamma\pi_i\delta^2 + w^2(\zeta_i\delta_r - \zeta_r\delta_i)}{(w+\gamma(w+1))\delta^2} - \frac{d\xi}{dw} \left[\frac{\delta_i(\eta_r + \pi_r) + \delta_r(\eta_i + \pi_i)}{(w+\gamma(w+1))} \right] \quad (35)$$

$$\frac{d\pi_r}{dw} = \frac{-\xi}{w} + \frac{(\delta_r\eta_r - \delta_i\eta_i)}{w} \frac{d\xi}{dw} + \frac{\eta_r}{w} + \frac{d\eta_r}{dw} - \frac{w(\zeta_r\delta_r + \zeta_i\delta_i)}{\delta^2} \quad (36)$$

$$\frac{d\pi_i}{dw} = \frac{(\delta_i\eta_r + \delta_r\eta_i)}{w} \frac{d\xi}{dw} + \frac{\eta_i}{w} + \frac{d\eta_i}{dw} - \frac{w(\zeta_i\delta_r - \zeta_r\delta_i)}{\delta^2} \quad (37)$$

$$\frac{d\zeta_r}{dw} = \frac{\xi\delta_r}{w^3} - \frac{d\xi}{dw} \frac{\zeta_r\delta_r}{w} + \frac{\delta_r}{w^2} \frac{d\eta_r}{dw} - \frac{\eta_r\delta_r}{w^3} - \frac{\delta_r(\zeta_r\delta_r + \zeta_i\delta_i)}{w\delta^2} + \frac{d\xi}{dw} \frac{\zeta_i\delta_i}{w} - \frac{\delta_i}{w^2} \frac{d\eta_i}{dw} + \frac{\eta_i\delta_i}{w^3} + \frac{\delta_i(\zeta_i\delta_r - \zeta_r\delta_i)}{w\delta^2} \quad (38)$$

$$\frac{d\zeta_i}{dw} = \frac{\xi\delta_i}{w^3} - \frac{d\xi}{dw} \frac{\zeta_i\delta_r}{w} + \frac{\delta_r}{w^2} \frac{d\eta_i}{dw} - \frac{\eta_i\delta_r}{w^3} - \frac{\delta_r(\zeta_i\delta_r - \zeta_r\delta_i)}{w\delta^2} - \frac{d\xi}{dw} \frac{\zeta_r\delta_i}{w} + \frac{\delta_i}{w^2} \frac{d\eta_r}{dw} - \frac{\eta_r\delta_i}{w^3} - \frac{\delta_i(\zeta_r\delta_r + \zeta_i\delta_i)}{w\delta^2} \quad (39)$$

There are three free parameters: α , β and γ . The quantities δ_r and δ_i are eigenvalues which are determined by imposing the boundary condition at the wall where $w = 0$ or the imaginary and real parts of the velocity, η_r and η_i vanish. This implies that $|\eta| = (\eta_i^2 + \eta_r^2)^{0.5} = 0$. We solved the differential equations employing a fourth order Runge-Kutta

technique for trial values of δ_r and δ_i with the combination that satisfies the boundary condition being the eigenvalue. We followed the method described by Saxton et al. (1998) which involves choosing a grid of points in the complex plane consisting of δ_r and δ_i and integrating the equations for each point on the grid. The value of $1/|\eta|$ is then plotted and the eigenvalues show up as sharp spikes. This is illustrated in Fig. 2 for a specific case. In our analysis we have used 250×250 points for (δ_i, δ_r) . Once we obtained the eigenvalues, the next step was to improve accuracy by selecting a smaller grid near the eigenvalue and repeating the above procedure. High accuracy is then reached as illustrated in Fig. 3.

3 GENERAL RESULTS

3.1 Stability

We have performed the stability analyses and computed frequencies for several cases of β and γ for various values of α . The results are recorded in Tables 1–8. In each table, we also present the critical value of α below which overstability sets in, in each case to three decimal places. The growth or damping rates are plotted in Figs. 4, 5, 6 and 7, where we immediately note that all shocks are unstable for α sufficiently low. Moreover, the critical values of α decrease as β decreases and/or γ decreases.

As a check, our values are consistent with previous results where overlapping in parameter space. We have also reproduced the results of CI82 with more accurate values for the eigenfrequencies. In particular, the critical value for the fundamental mode, $\alpha_c = 0.388$, for the well-studied case $\gamma = 5/3$ and $\beta = 2$ is in agreement with Imamura et al. (1996) who derived a value of 0.39.

For a pure diatomic gas, the instability regime of the fundamental mode is significantly more restricted, e.g. $\alpha_c = -0.241$ for $\beta = 2$. *Negative values of the temperature index α are necessary for molecular shocks whereas positive values can be sufficient for atomic shocks.* For the higher modes, however, the difference is less dramatic. As an example, for the $\beta = 2$ case, the first overtone is unstable for $\alpha < 0.782$ and $\alpha < 0.663$ for $\gamma = 5/3$ and $\gamma = 7/5$, respectively.

The fundamental mode possesses a more restricted instability regime than the associated overtones in all cases. However, note that, with the exception of the $\beta = 2$ and $\gamma = 5/3$ case, the instability regime generally does not increase as the eigenmode number increases. It is evident from the tables that the second overtone is generally stable in a wider regime than either the first or third overtone. In addition, the contrary holds in the $\beta = 2$ and $\gamma = 21/19$ case.

The density dependence of the cooling, measured by β , has a strong influence on the onset of instability. As discussed by Imamura et al. (1996), $\beta - \alpha$ plays an important role rather than α or β independently. This can be seen to originate from the forms of equations (34) and (35) and reflects the fact that the total pressure variation across the cooling layer is relatively small in comparison to the mammoth compression. This is confirmed in Figs. 4–7 where the difference in growth rates between $\beta = 1$ and $\beta = 2$ is illustrated for various values of γ : as γ decreases, the direct

dependence on $\beta - \alpha$ becomes stronger. This is most evident for the case $\gamma = 21/19$, where the dependence is effectively only on $\beta - \alpha$ while the pressure variation between the shocked gas and the wall is only $\rho_a u_{in}^2/20$.

We note that for the case $\beta = 1$ and $\gamma = 5/3$, with $\alpha = 0.5$, our third overtone mode is the second overtone reported by Imamura (1985). For $\alpha = 1$, we find that, except for the fundamental mode, our results are quite different. For example, our second overtone corresponds to Imamura's first overtone. The reason is that if the modes have similar growth rates and frequencies, one can easily miss modes. Therefore the resolution is very important in order not to overlook modes.

3.2 Oscillation period

We find that the eigenvalues (δ_i) often show a pattern that resembles acoustic modes within a pipe with one end closed. Accordingly, the frequencies are represented by

$$\delta_i = \delta_s \left(n - \frac{1}{2} \right) + \delta_c,$$

where n is a positive integer, the frequency spacing between the modes is represented by δ_s and δ_c is the correction required to fit exactly a pipe with one end closed. We present the values of δ_s and δ_c for the various modes in Tables 9–12.

For the case $\gamma = 5/3$, this pattern is also exhibited when the cooling is made up of multiple processes, consisting of bremsstrahlung and a destabilizing process (Saxton et al. 1998). Such a pattern was also reported in the presence of a transverse magnetic field (Toth & Draine 1993). Here, we add that this behaviour is generally true.

Note that the correction factors are relatively small for the case $\gamma = 21/19$, suggesting that the pipe analogy is most appropriate when the pressure change in the cooling layer is least. In general however, the pipe analogy is inappropriate when $\beta \sim \alpha$.

We find that the eigenfrequencies show a similar functional dependence on $\beta - \alpha$, as displayed in Figs. 8–11, for the various cases of γ . It is also seen that the frequency behaviour does roughly approach a constant at high values of $\beta - \alpha$, although an asymptotic limit is only discernible in the fundamental mode with γ near unity. Overall, it is evident from the plots that increasing the value of γ increases the eigenfrequency for corresponding values of β and α . This is especially clear for all the overtones. This is at least partly because the post-shock gas is hotter for higher values of γ , allowing sound waves to propagate faster.

4 DISCUSSION: MOLECULAR SHOCK

A gas composed predominantly of molecular hydrogen may possess various effective specific heat ratios which may vary through the shock as the translation, vibrational, and rotational degrees of freedom are activated. In cold H_2 gas, $\gamma = 5/3$ is appropriate since it behaves as a monatomic gas. Where rotational modes become excited, $\gamma = 7/5$ since diatomic molecules have 2 rotational degrees of freedom. In astrophysical contexts there is invariably an additional 10% of helium atoms which raises the value to $\gamma = 10/7$. At temperatures exceeding a few thousand Kelvin, vibrational

Table 1. Eigenfrequencies and critical stability values for parameters $\gamma = 5/3$ and $\beta = 1$.

	fundamental ($\alpha_c = 0.051$)		first overtone ($\alpha_c = 0.149$)		second overtone ($\alpha_c = 0.028$)		third overtone ($\alpha_c = 0.147$)	
α	δ_r	δ_i	δ_r	δ_i	δ_r	δ_i	δ_r	δ_i
-2	0.2199	0.2452	0.3614	0.9077	0.3915	1.6508	0.4253	2.3334
-1	0.1239	0.3122	0.2150	0.8946	0.2310	1.5625	0.2690	2.1856
-0.5	0.0719	0.3378	0.1323	0.8662	0.1328	1.4782	0.1729	2.0557
0	0.0078	0.3595	0.0339	0.8085	0.0082	1.3347	0.0478	1.8501
0.5	-0.0936	0.3688	-0.0886	0.6826	-0.1616	1.0425	-0.1674	1.4606
1	-0.5254	0.2490	-0.5606	0.4650	-0.1490	0.6133	-0.5783	0.6685

Table 2. Eigenfrequencies and critical stability values for parameters $\gamma = 5/3$ and $\beta = 2$

	fundamental ($\alpha_c = 0.388$)		first overtone ($\alpha_c = 0.782$)		second overtone ($\alpha_c = 0.795$)		third overtone ($\alpha_c = 0.882$)	
α	δ_r	δ_i	δ_r	δ_i	δ_r	δ_i	δ_r	δ_i
-2	0.1671	0.2175	0.3443	0.9581	0.3905	1.7252	0.4258	2.4622
-1	0.1031	0.2616	0.2393	0.9510	0.2786	1.6778	0.3121	2.3820
-0.5	0.0684	0.2787	0.1827	0.9399	0.2161	1.6398	0.2477	2.3204
0	0.0323	0.2934	0.1202	0.9210	0.1450	1.5857	0.1739	2.2347
0.5	-0.0102	0.3052	0.0476	0.8887	0.0602	1.5043	0.0851	2.1087
1	-0.0622	0.3121	-0.0420	0.8307	-0.0485	1.3698	-0.0310	1.9069

modes become relevant; there are two degrees of freedom per vibrational mode yielding $\gamma = 9/7$ for pure H_2 .

The cooling function may take many forms depending on the density temperature and history of the gas (e.g., SR03). Above critical densities, collisions determine the relevant energy levels of the radiating particles. Thus, they approach thermodynamic equilibrium and $\beta = 1$. At lower density, each exciting collision leads to the emission of a photon and so $\beta = 2$.

Will molecular shocks be unstable? We might expect molecular shocks to be stable to the fundamental mode since derived power-law cooling approximations to components of the cooling function yield values of α near unity whereas the instability requires negative α . For example, molecular hydrogen ro-vibrational cooling is a strong positive function of α below 4000 K, with $\alpha \sim 3$ to 5. Above 4000 K, however, $\alpha \sim 0.6$ to 1.0 with the lower values arising under high density conditions (Le Bourlot et al. 1999). Cooling through rotational excitation of H_2O , OH and CO are also represented by power laws exceeding unity (see summary presented by SR03). For CO vibrational cooling, however, the index approaches 0.5 at high temperature.

Oxygen and carbon fine-structure cooling is significant at temperatures below a few hundred Kelvin and can be dominant in circumstellar disks (Kamp & van Zadelhoff 2001). At densities exceeding $n_{\text{cr}}^{\text{H}} = 8.5 \times 10^5 (T/100)^{-0.69} \text{ cm}^{-3}$, LTE is a good approximation for the level populations of [O I]. At low temperatures, the cooling is then $\propto \exp(-228/T)$ while at sufficiently high temperature the index approaches zero. In the non-LTE case, $\alpha \sim 0.31$ to 0.35 when collisionally excited by H_2 (e.g., SR03). Hence, we predict that in this latter case a molecular shock would be linearly unstable to first and higher order modes (on comparison to the critical values given in Table 6).

The formation of trace molecules within a shock can considerably enhance the cooling rate as the gas cools – the conditions needed to promote the fundamental mode of the instability. In the molecular case, a non-dissociative shock which raises the gas temperature above ~ 300 K would instigate the formation of H_2O . Assuming that the oxygen in the pre-shock medium is atomic or tied up in grains or CO, as the molecules form the cooling rate increases. As the temperature begins to fall, however, the rate of formation of further molecules is drastically reduced. Hence, it is unclear if this will lead to instability.

Fast dissociative shocks possess a regime of instability, as discussed in § 1. The hydrogen is converted into atomic form in the hot shock front. The delayed reformation of a small fraction of H_2 suffices to seed the formation of CO and H_2O . This generates two bumps in the cooling function experienced by a parcel of gas, caused by vibrational cooling of these molecules. However, since the shock is dissociative, strong atomic cooling occurs immediately behind the shock front. This cooling takes place in a narrow layer and, as illustrated here by the case $\gamma = 21/19$, provides a barrier to the instability. The shock front conditions resembles that of a shock with γ near unity. As demonstrated by the case $\gamma = 21/19$, the instability condition in the subsequent cooling layer becomes significantly more stringent.

5 CONCLUSIONS: MOLECULAR SHOCK

We have investigated the stability of radiative shocks for a range of specific heat ratios and cooling functions represented by power-law functions of temperature and density. Our major results are as follows.

Table 3. Eigenfrequencies and critical stability values for parameters $\gamma = 7/5$ and $\beta = 1$

α	fundamental ($\alpha_c = -0.532$)		first overtone ($\alpha_c = 0.072$)		second overtone ($\alpha_c = -0.208$)		third overtone ($\alpha_c = -0.028$)	
	δ_r	δ_i	δ_r	δ_i	δ_r	δ_i	δ_r	δ_i
-2	0.0726	0.2089	0.1952	0.6803	0.1947	1.2211	0.2476	1.7278
-1	0.0272	0.2322	0.1177	0.6550	0.1022	1.1370	0.1551	1.6092
-0.5	-0.0021	0.2425	0.0684	0.6299	0.0419	1.0634	0.0904	1.5112
0	-0.0408	0.2493	0.0101	0.5874	-0.0334	0.9426	-0.0070	1.3549
0.5	-0.1017	0.2403	-0.0758	0.5094	-0.1195	0.7142	-0.1642	1.0192
1	-0.3603	0.1473	-0.3923	0.2926	-0.4084	0.4332	-0.1075	0.5099

Table 4. Eigenfrequencies and critical stability values for parameters $\gamma = 7/5$ and $\beta = 2$

α	fundamental ($\alpha_c = -0.241$)		first overtone ($\alpha_c = 0.663$)		second overtone ($\alpha_c = 0.592$)		third overtone ($\alpha_c = 0.774$)	
	δ_r	δ_i	δ_r	δ_i	δ_r	δ_i	δ_r	δ_i
-2	0.0616	0.1814	0.1896	0.7093	0.2126	1.2738	0.2516	1.8147
-1	0.0295	0.1986	0.1330	0.6953	0.1495	1.2288	0.1867	1.7456
-0.5	0.0108	0.2064	0.1000	0.6833	0.1115	1.1951	0.1474	1.6948
0	-0.0007	0.2134	0.0621	0.6655	0.0666	1.1484	0.1006	1.6258
0.5	-0.0366	0.2190	0.0170	0.6379	0.0117	1.0795	0.0412	1.5264
1	-0.0698	0.2210	-0.0402	0.5918	-0.0586	0.9676	-0.0422	1.3690

Decreasing the specific heat ratio leads to a significantly more restricted range of instability for the fundamental mode. Since this mode could lead to large-scale non-linear disturbances, molecular shocks can be considered to be more stable than atomic shocks. This result contrasts with the dynamical overstability of Vishniac (1983), which generates ripples across the shock front that grow as a power law with time. This instability is more prominent for lower effective specific heat ratios (e.g. Grun et al. 1991; Laming & Grun 2002) i.e when the shock wave is sufficiently thin (Mac Low & Norman 1993).

The harmonics, however, show much less dependence on γ , suggesting that higher frequency modes are particularly important for molecular shocks.

There is a strong dependence of the instability on $\beta - \alpha$ rather than on the parameters independently. There is a particularly tight relationship for lower values of γ .

There is no set of conditions where hydrodynamic shocks are fully steady and stable. Firstly, the total shock length is infinite for $\alpha > 1 + \beta$. Secondly, shocks never reach a steady state for $\alpha > \beta$. Thirdly, small upstream disturbances would be amplified in the cooling layer through the thermal instability for $\alpha < \beta$, although some damping may occur near the shock front (Smith 1989). Fourthly, the overstability leads to growing oscillations for $\alpha < \alpha_c$.

With the ability to detect emission from a wide range of molecules, shocks propagating through molecular gas are becoming increasingly observed. The signature attributable to the overstability would perhaps correspond to rapidly growing oscillations. The general signature is that of a 'periodic shock'. Such behaviour has been suggested to explain the 22 GHz water maser emission in VY CMa (Wu Zheng et al. 1998). In this case, a quasi-sinusoidal fluctuation was de-

tected with the relative flux intensity change of 20%-25% and a period of 10.3 day for two dominant features.

However, whether or not the overstability generates observable phenomena will depend on other factors such as the magnetic field direction and strength. In addition, gas in molecular clouds will be shielded from ionising radiation. A low ion fraction allows ion-magnetosonic waves to propagate ahead of the shock front, altering the shock structure (Draine et al. 1983) and the stability properties (Wardle 1991). Therefore, much will depend on the environment of the shock wave. The multi-dimensional structure and non-linear properties will also greatly influence the signatures especially of the higher harmonics which possess shorter wavelengths. One potential occurrence discussed in § 4 is related to molecular shocks which raise the gas above about 300 K.

ACKNOWLEDGMENTS

Research at Armagh Observatory is funded by the Department of Culture, Arts and Leisure, Northern Ireland. BR is extremely grateful to Sathya Sai Baba for encouragement and also thanks Ignacio Ugarte-Urra and Lidong Xia for useful discussions. BR also thanks Professor Mark Bailey for encouragement.

REFERENCES

- Bertschinger E., 1986, ApJ, 304, 154
- Birnboim Y., Dekel A., 2003, MNRAS, 345, 349
- Chevalier R. A., Imamura J. N., 1982, ApJ, 261, 543
- Dgani R., Soker N., 1994, ApJ, 434, 262

Table 5. Eigenfrequencies and critical stability values for parameters $\gamma = 10/7$ and $\beta = 1$

fundamental ($\alpha_c = -0.432$)		first overtone ($\alpha_c = 0.085$)		second overtone ($\alpha_c = -0.176$)		third overtone ($\alpha_c = 0.003$)		
α	δ_r	δ_i	δ_r	δ_i	δ_r	δ_i	δ_r	δ_i
-2	0.0855	0.2162	0.2115	0.7097	0.2146	1.2772	0.2661	1.8034
-1	0.0362	0.2426	0.1277	0.6844	0.1152	1.1914	0.1681	1.6803
-0.5	0.0048	0.2542	0.0762	0.6586	0.0505	1.1158	0.1007	1.5785
0	-0.0365	0.2625	0.0126	0.6139	-0.0300	0.9911	0.0008	1.4174
0.5	-0.1020	0.2552	-0.0764	0.5306	-0.1263	0.7532	-0.1674	1.0746
1	-0.3791	0.1591	-0.4118	0.3122	-0.4284	0.4601	-0.1142	0.5238

Table 6. Eigenfrequencies and critical stability values for parameters $\gamma = 10/7$ and $\beta = 2$

fundamental ($\alpha_c = -0.134$)		first overtone ($\alpha_c = 0.680$)		second overtone ($\alpha_c = 0.623$)		third overtone ($\alpha_c = 0.794$)		
α	δ_r	δ_i	δ_r	δ_i	δ_r	δ_i	δ_r	δ_i
-2	0.0714	0.1875	0.2051	0.7408	0.2312	1.3315	0.2697	1.8959
-1	0.0366	0.2067	0.1439	0.7270	0.1634	1.2856	0.1966	1.8167
-0.5	0.0166	0.2154	0.1086	0.7149	0.1227	1.2511	0.1583	1.7722
0	-0.0066	0.2231	0.0681	0.6967	0.0750	1.2033	0.1084	1.7007
0.5	-0.0342	0.2294	0.0199	0.6683	0.0166	1.1324	0.0466	1.5977
1	-0.0693	0.2319	-0.0407	0.6192	-0.0585	1.0172	-0.0401	1.4349

Dgani R., van Buren D., Noriega-Crespo A., 1996, ApJ, 461, 927
 Draine B. T., McKee C. F., 1993, ARA&A, 31, 373
 Draine B. T., Roberge W. G., Dalgarno A., 1983, ApJ, 264, 485
 Fesen R. A., Kwitter K. B., Downes R. A., 1992, AJ, 104, 719
 Fischer A., Beuermann K., 2001, A&A, 373, 211
 Grun J., Stamper J., Manka C., Resnick J., Burris R., 1991, Physical Review Letters, 66, 2738
 Hartigan P., Raymond J., Hartmann L., 1987, ApJ, 316, 323
 Hollenbach D., McKee C. F., 1989, ApJ, 342, 306
 Houck J. C., Chevalier R. A., 1992, ApJ, 395, 592
 Imamura J. N., 1985, ApJ, 296, 128
 Imamura J. N., Aboasha A., Wolff M. T., Wood K. S., 1996, ApJ, 458, 327
 Imamura J. N., Wolff M. T., Durisen R. H., 1984, ApJ, 276, 667
 Kamp I., van Zadelhoff G.-J., 2001, A&A, 373, 641
 Laming J. M., Grun J., 2002, Physical Review Letters, 89, 125002
 Langer S. H., Chanmugam G., Shaviv G., 1981, ApJ, 245, L23
 Larsson S., 1992, A&A, 265, 133
 Le Bourlot J., Pineau des Forêts G., Flower D. R., 1999, MNRAS, 305, 802
 Lesaffre P., Chièze J.-P., Cabrit S., Pineau des Forêts G., 2004, A&A, p. in press
 Mac Low M., Norman M. L., 1993, ApJ, 407, 207
 McKee C. F., Hollenbach D. J., 1980, ARA&A, 18, 219
 Saxton C. J., Wu K., Pongracic H., Shaviv G., 1998, MNRAS, 299, 862
 Smith M. D., 1989, MNRAS, 238, 235

Smith M. D., Rosen A., 2003, MNRAS, 339, 133
 Strickland R., Blondin J. M., 1995, ApJ, 449, 727
 Sutherland R. S., Bicknell G. V., Dopita M. A., 2003, ApJ, 591, 238
 Toth G., Draine B. T., 1993, ApJ, 413, 176
 Vishniac E. T., 1983, ApJ, 274, 152
 Vishniac E. T., 1994, ApJ, 428, 186
 Wardle M., 1991, MNRAS, 250, 523
 Wolff M. T., Wood K. S., Imamura J. N., Middleditch J., Steiman-Cameron T. Y., 1999, ApJ, 526, 435
 Wu Zheng X., Scalise E. J., Han F., 1998, ApJ, 507, 384

APPENDIX A: BOUNDARY CONDITIONS AT THE MOVING SHOCK

In the steady state case, both the incoming gas and the outgoing gas (at the shock) are the same for a stationary observer as well as the shock. But the situation changes when the shock starts oscillating. Now the stationary observer will find the same incoming velocity with a different velocity for the post-shock gas which consists of two parts, viz, the steady state velocity and a small perturbed term which will be determined as follows. Let the velocity of the shock be $v_s = v_{s1} e^{\sigma t}$ according to the stationary observer. In the frame of the shock,

$$v_{in} = -u_{in} - v_s \quad (\text{A1})$$

where v_{in} is the incoming gas velocity. If v is the velocity of the post-shock gas in the observer frame, it implies that $v - v_s$ will be the velocity as seen from the shock frame.

Table 7. Eigenfrequencies and critical stability values for parameters $\gamma = 21/19$ and $\beta = 1$

	fundamental ($\alpha_c = -4.874$)		first overtone ($\alpha_c = -0.702$)		second overtone ($\alpha_c = -0.318$)		third overtone ($\alpha_c = -1.020$)	
α	δ_r	δ_i	δ_r	δ_i	δ_r	δ_i	δ_r	δ_i
-2	-0.0214	0.0835	0.0327	0.2694	0.0358	0.4306	0.0271	0.6366
-1	-0.0332	0.0846	0.0095	0.2578	0.0161	0.3953	-0.0006	0.5777
-0.5	-0.0408	0.0835	-0.0077	0.2471	0.0045	0.3675	-0.0186	0.5290
0	-0.0501	0.0797	-0.0328	0.2270	-0.0084	0.3293	-0.0391	0.4534
0.5	-0.0606	0.0679	-0.0673	0.1766	-0.0446	0.2850	-0.0450	0.3189
1	-0.1311	0.0323	-0.1402	0.0816	-0.1449	0.1264	-0.1454	0.1696

Table 8. Eigenfrequencies and critical stability values for parameters $\gamma = 21/19$ and $\beta = 2$

	fundamental ($\alpha_c = -4.692$)		first overtone ($\alpha_c = -0.026$)		second overtone ($\alpha_c = 0.240$)		third overtone ($\alpha_c = -0.118$)	
α	δ_r	δ_i	δ_r	δ_i	δ_r	δ_i	δ_r	δ_i
-2	-0.0163	0.0778	0.0362	0.2721	0.0426	0.4571	0.0426	0.6708
-1	-0.0250	0.0796	0.0208	0.2647	0.0268	0.4365	0.0231	0.6377
-0.5	-0.0303	0.0802	0.0111	0.2592	0.0171	0.4215	0.0109	0.6135
0	-0.0366	0.0802	-0.0007	0.2514	0.0060	0.4016	-0.0037	0.5806
0.5	-0.0440	0.0791	-0.0159	0.2396	-0.0071	0.3738	-0.0213	0.5334
1	-0.0530	0.0754	-0.0372	0.2192	-0.0231	0.3331	-0.0418	0.4604

Applying the Rankine-Hugoniot condition, we get

$$v - v_s = \left(\frac{\gamma - 1}{\gamma + 1} \right) v_{in} \quad (\text{A2})$$

Rearranging the terms, we obtain

$$v = -u_{in} \left(\frac{\gamma - 1}{\gamma + 1} \right) + \frac{2v_s}{\gamma + 1} \quad (\text{A3})$$

Comparing this with equation (23) we find that that the perturbed velocity is

$$v_1 = \frac{2v_{s1}}{\gamma + 1} \quad (\text{A4})$$

Now for the perturbation in density, we use the Rankine-Hugoniot condition which expresses the conservation of mass, viz,

$$\rho_{in} v_{in} = \rho (v - v_s) \quad (\text{A5})$$

where ρ_{in} and ρ are the pre-shock and post-shock densities and $\rho_{in} = \rho_a$. Then equation (A2) implies that

$$\rho = \rho_a \left(\frac{\gamma + 1}{\gamma - 1} \right) \quad (\text{A6})$$

which is identical to the steady state condition. Therefore, there is no perturbation term for density or $\rho_1 = 0$.

For the pressure perturbation, we use the Rankine-Hugoniot condition for the conservation of momentum flux. Neglecting the pre-shock pressure of the gas and denoting p as the post-shocked gas pressure,

$$p = \rho_{in} v_{in}^2 - \rho (v - v_s)^2 \quad (\text{A7})$$

Substituting for the expression for ρ from above, we find

$$p = \frac{2\rho_{in} u_{in}^2}{\gamma + 1} + \frac{4\rho_{in} u_{in} v_s}{\gamma + 1} \quad (\text{A8})$$

which implies from equation (22) that the perturbed part of the pressure is

$$p_1 = \left(\frac{4\rho_a u_{in} v_{s1}}{\gamma + 1} \right). \quad (\text{A9})$$

APPENDIX B: ANALYTICAL SOLUTIONS FOR STEADY SHOCKS

Here we present the analytical steady state solutions for ξ by integrating eq. (13) for various values of α and β . The solutions are expressed in terms of γ . We use the notation $\xi_{\alpha, \beta}$ to indicate the specific case of α and β . In the paper of Imamura (1985), there seems to be a typographical error for the case of $\alpha = -1$.

Table 9. Frequency spacing (δ_s) and correction (δ_c) for $\gamma = 5/3$.

α	$\beta = 1$						$\beta = 2$					
	first overtone		second overtone		third overtone		first overtone		second overtone		third overtone	
	δ_s	δ_c	δ_s	δ_c	δ_s	δ_c	δ_s	δ_c	δ_s	δ_c	δ_s	δ_c
-2	0.6625	-0.0861	0.7431	-0.2070	0.6826	-0.0557	0.7406	-0.1528	0.7671	-0.1926	0.7370	-0.1173
-1	0.5824	0.0210	0.6679	-0.1073	0.6231	0.0048	0.6894	-0.0831	0.7268	-0.1392	0.7042	-0.0827
-0.5	0.5284	0.0736	0.6120	-0.0518	0.5775	0.0345	0.6612	-0.0519	0.6999	-0.1100	0.6806	-0.0617
0	0.4490	0.1350	0.5262	0.0192	0.5154	0.0462	0.6276	-0.0204	0.6647	-0.0761	0.6490	-0.0368
0.5	0.3138	0.2119	0.3599	0.1428	0.4181	-0.0028	0.5835	0.0135	0.6156	-0.0347	0.6044	-0.0067
1	0.2160	0.1410	0.1483	0.2426	0.0552	0.4753	0.5186	0.0528	0.5391	0.0221	0.5371	0.0271

Table 10. Frequency spacing (δ_s) and correction (δ_c) for $\gamma = 7/5$.

α	$\beta = 1$						$\beta = 2$					
	first overtone		second overtone		third overtone		first overtone		second overtone		third overtone	
	δ_s	δ_c	δ_s	δ_c	δ_s	δ_c	δ_s	δ_c	δ_s	δ_c	δ_s	δ_c
-2	0.4714	-0.0268	0.5408	-0.1309	0.5067	-0.0457	0.5279	-0.0826	0.5645	-0.1375	0.5409	-0.0785
-1	0.4228	0.0208	0.4820	-0.0608	0.4772	-0.0435	0.4967	-0.0498	0.5335	-0.1050	0.5168	-0.0632
-0.5	0.3874	0.0488	0.4335	-0.0204	0.4478	-0.0561	0.4769	-0.0321	0.5118	-0.0844	0.4997	-0.0542
0	0.3381	0.0803	0.3552	0.0546	0.4123	-0.0882	0.4521	-0.0127	0.4829	-0.0589	0.4774	-0.0451
0.5	0.2691	0.1058	0.2048	0.2022	0.3050	-0.0483	0.4189	0.0096	0.4416	-0.0245	0.4469	-0.0378
1	0.1453	0.0747	0.1406	0.0817	0.0767	0.2415	0.3708	0.0356	0.3758	0.0281	0.4014	-0.0359

Table 11. Frequency spacing (δ_s) and correction (δ_c) for $\gamma = 10/7$.

α	$\beta = 1$						$\beta = 2$					
	first overtone		second overtone		third overtone		first overtone		second overtone		third overtone	
	δ_s	δ_c	δ_s	δ_c	δ_s	δ_c	δ_s	δ_c	δ_s	δ_c	δ_s	δ_c
-2	0.4935	-0.0306	0.5675	-0.1916	0.5262	-0.0383	0.5533	-0.0892	0.5907	-0.1453	0.5644	-0.0795
-1	0.4418	0.0217	0.5070	-0.0761	0.4889	-0.0309	0.5203	-0.0535	0.5586	-0.1109	0.5311	-0.0422
-0.5	0.4044	0.0520	0.4572	-0.0272	0.4627	-0.0410	0.4995	-0.0344	0.5362	-0.0894	0.5211	-0.0517
0	0.3514	0.0868	0.3772	0.0481	0.4263	-0.0747	0.4736	-0.0137	0.5066	-0.0632	0.4974	-0.0402
0.5	0.2754	0.1175	0.2226	0.1967	0.3214	-0.0503	0.4389	0.0100	0.4641	-0.0276	0.4653	-0.0309
1	0.1531	0.0826	0.1479	0.0904	0.0637	0.3009	0.3873	0.0383	0.3980	0.0222	0.4177	-0.0271

Table 12. Frequency spacing (δ_s) and correction (δ_c) for $\gamma = 21/19$.

α	$\beta = 1$						$\beta = 2$					
	first overtone		second overtone		third overtone		first overtone		second overtone		third overtone	
	δ_s	δ_c	δ_s	δ_c	δ_s	δ_c	δ_s	δ_c	δ_s	δ_c	δ_s	δ_c
-2	0.1859	-0.0095	0.1612	0.0276	0.2060	-0.0844	0.1943	-0.0194	0.1850	-0.0054	0.2137	-0.0772
-1	0.1732	-0.0002	0.1375	0.0516	0.1824	-0.0607	0.1851	-0.0130	0.1718	0.0070	0.2012	-0.0665
-0.5	0.1636	0.0061	0.1204	0.0665	0.1615	-0.0363	0.1790	-0.0093	0.1623	0.0158	0.1920	-0.0585
0	0.1473	0.0061	0.1023	0.0736	0.1241	0.0191	0.1712	-0.0054	0.1502	0.0261	0.1790	-0.0459
0.5	0.1087	0.0136	0.1084	0.0140	0.0339	0.2003	0.1605	-0.0012	0.1342	0.0383	0.1596	-0.0252
1	0.0493	0.0077	0.0448	0.0144	0.0432	0.0184	0.1438	0.0035	0.1139	0.0484	0.1273	-0.0149

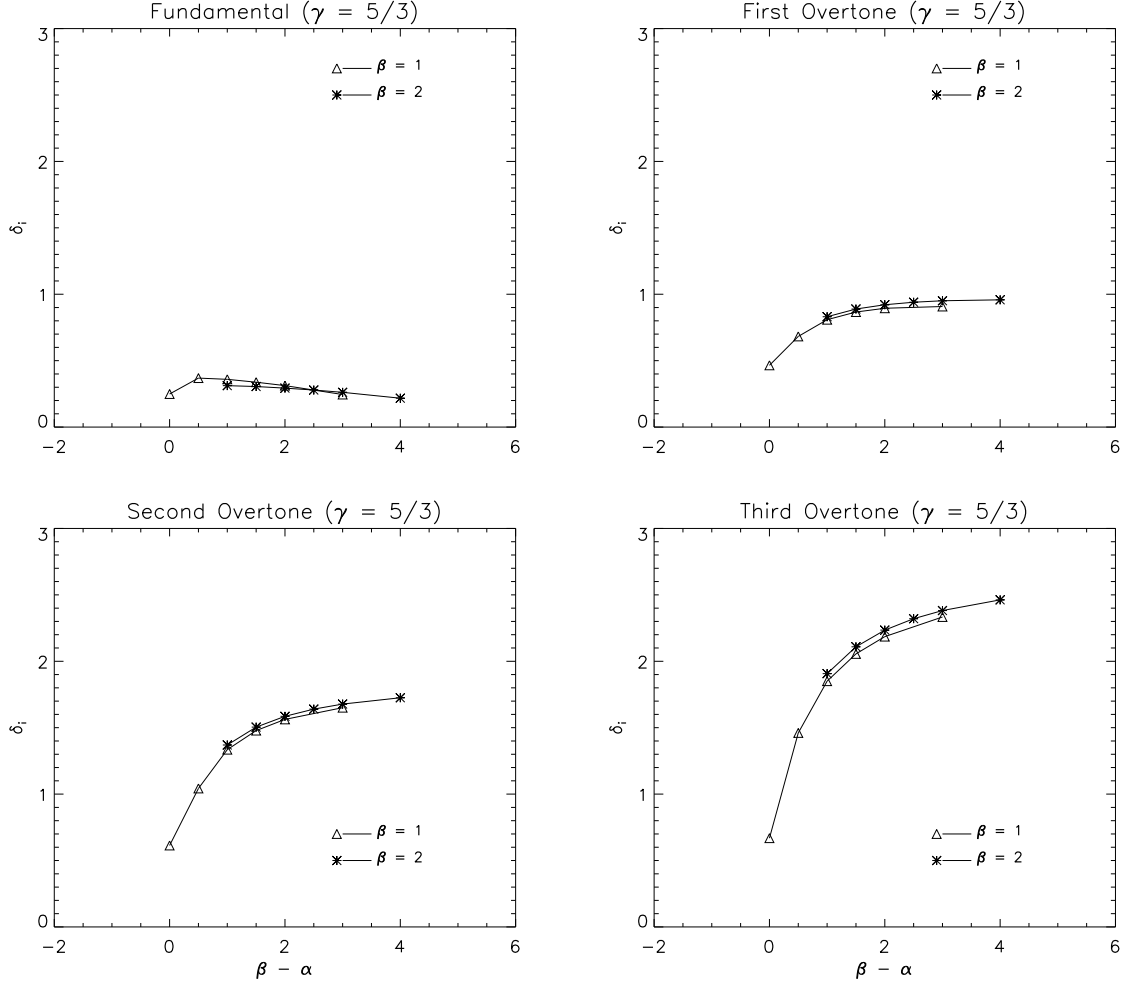


Figure 8. The frequency δ_i is plotted versus $\beta - \alpha$ ($\gamma = 5/3$) for various modes.

$$\xi_{-2,1} = \left[\frac{(\gamma+1)w^3}{7} + \frac{(2+3\gamma)w^2}{6} + \frac{w(1+3\gamma)}{5} + \frac{\gamma}{4} \right] \times \frac{420w^4(\gamma+1)^6}{(\gamma-1)^4(3\gamma^3+26\gamma^2+107\gamma+284)} \quad (\text{B1})$$

$$\xi_{-1,1} = \left[\frac{(1+\gamma)w^2}{5} + \frac{(1+2\gamma)w}{4} + \frac{\gamma}{3} \right] \times \frac{60w^3(\gamma+1)^4}{(1-\gamma)^3(2\gamma^2+11\gamma+27)} \quad (\text{B2})$$

$$\xi_{0,1} = \left[\frac{(1+\gamma)w}{3} + \frac{\gamma}{2} \right] \times \left[\frac{6(\gamma+1)^2w^2}{(\gamma-1)^2(\gamma+2)} \right] \quad (\text{B3})$$

$$\xi_{1/2,1} = \left[\frac{1}{(2\gamma-2)^{1/2} + \frac{(3-\gamma)}{2} \left(\sin^{-1}\left(\frac{3-\gamma}{1+\gamma}\right) - \frac{\pi}{2} \right)} \right] \times \left((-w-w^2)^{1/2}(-2w-2w\gamma+3-\gamma) + \frac{(3-\gamma)}{2} \left[\sin^{-1}(2w+1) - \frac{\pi}{2} \right] \right) \quad (\text{B4})$$

$$\xi_{1,1} = [\ln(1+w) - w(1+\gamma)] \times \frac{1}{(\gamma-1) + \ln\left[\frac{2}{\gamma+1}\right]} \quad (\text{B5})$$

$$\xi_{-2,2} = \left[\frac{(\gamma+1)w^3}{8} + \frac{(2+3\gamma)w^2}{7} + \frac{w(1+3\gamma)}{6} + \frac{\gamma}{5} \right] \times \frac{840w^5(\gamma+1)^7}{(1-\gamma)^5(3\gamma^3+31\gamma^2+153\gamma+485)} \quad (\text{B6})$$

$$\xi_{-1,2} = \left[\frac{(1+\gamma)w^2}{6} + \frac{(1+2\gamma)w}{5} + \frac{\gamma}{4} \right] \times \frac{60w^4(\gamma+1)^5}{(1-\gamma)^4(\gamma^2+7\gamma+22)} \quad (\text{B7})$$

$$\xi_{0,2} = \left[\frac{(1+\gamma)w}{4} + \frac{\gamma}{3} \right] \times \left[\frac{12(\gamma+1)^3w^3}{(1-\gamma)^3(\gamma+3)} \right] \quad (\text{B8})$$

$$\xi_{1/2,2} = \left[\frac{1}{\frac{(2\gamma-2)^{1/2}(\gamma^2+16\gamma+23)}{(\gamma+1)^2} + \frac{(5-\gamma)}{2} \left(\sin^{-1}\left(\frac{3-\gamma}{1+\gamma}\right) - \frac{\pi}{2} \right)} \right] \times \left((-w-w^2)^{1/2}(8w^2(\gamma+1) + (\gamma-5)(2w-5)) + \frac{(5-\gamma)}{2} \left[\sin^{-1}(2w+1) - \frac{\pi}{2} \right] \right) \quad (\text{B9})$$

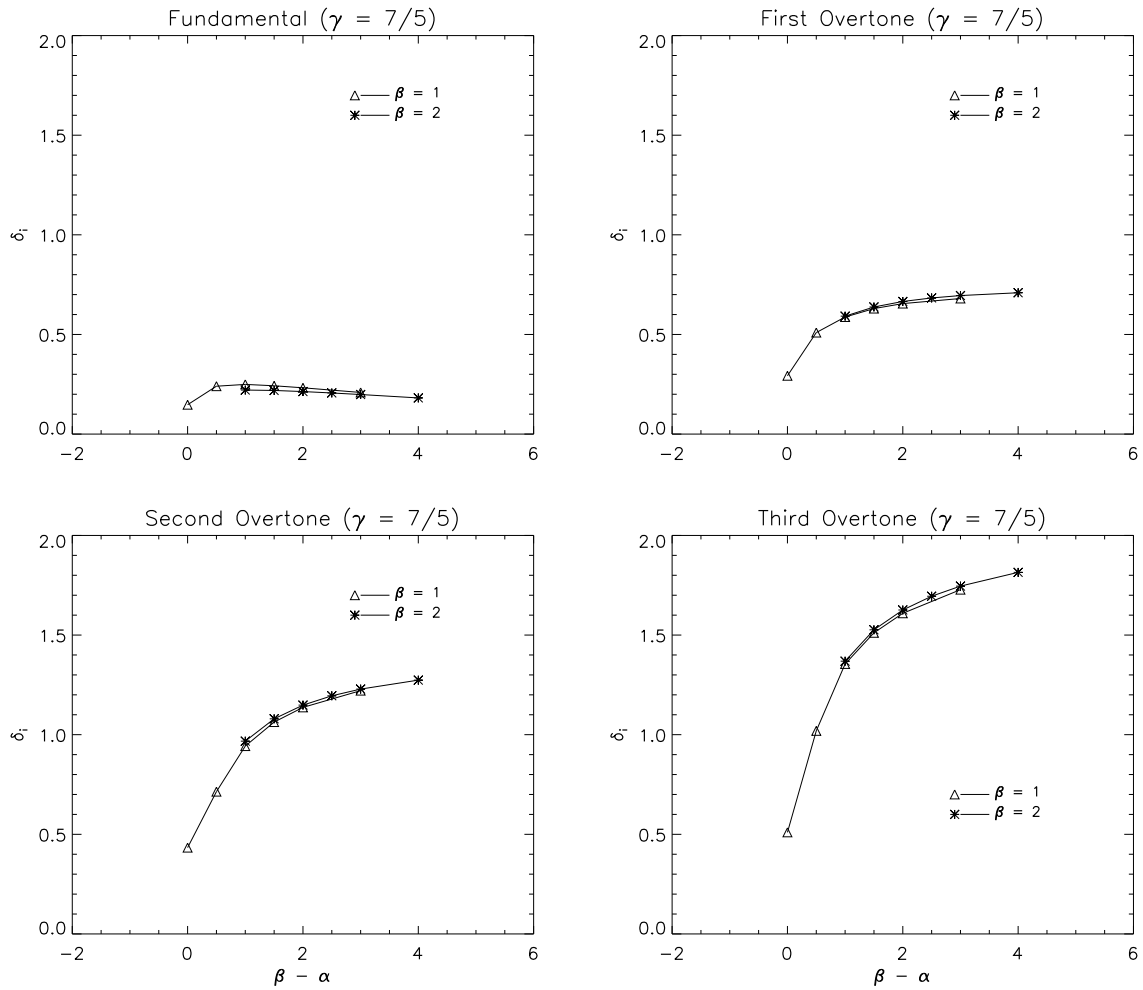


Figure 9. The frequency δ_i is plotted versus $\beta - \alpha$ ($\gamma = 7/5$) for various modes.

$$\xi_{1,2} = \frac{\left[\frac{(1+\gamma)w^2}{2} - w + \ln(1+w) \right]}{\frac{(\gamma-1)}{2} + \ln \left[\frac{2}{\gamma+1} \right]} \quad (\text{B10})$$

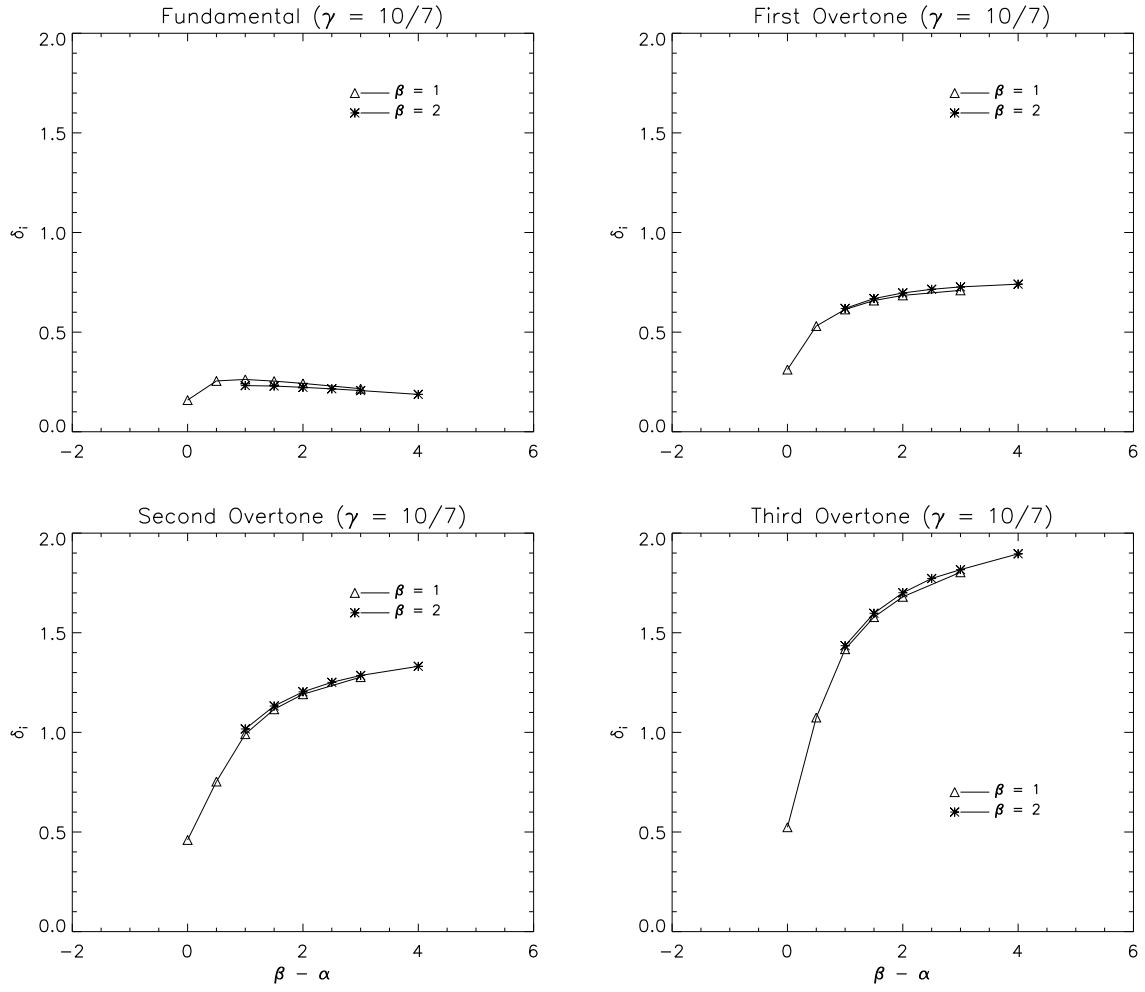


Figure 10. The frequency δ_i is plotted versus $\beta - \alpha$ ($\gamma = 10/7$) for various modes.

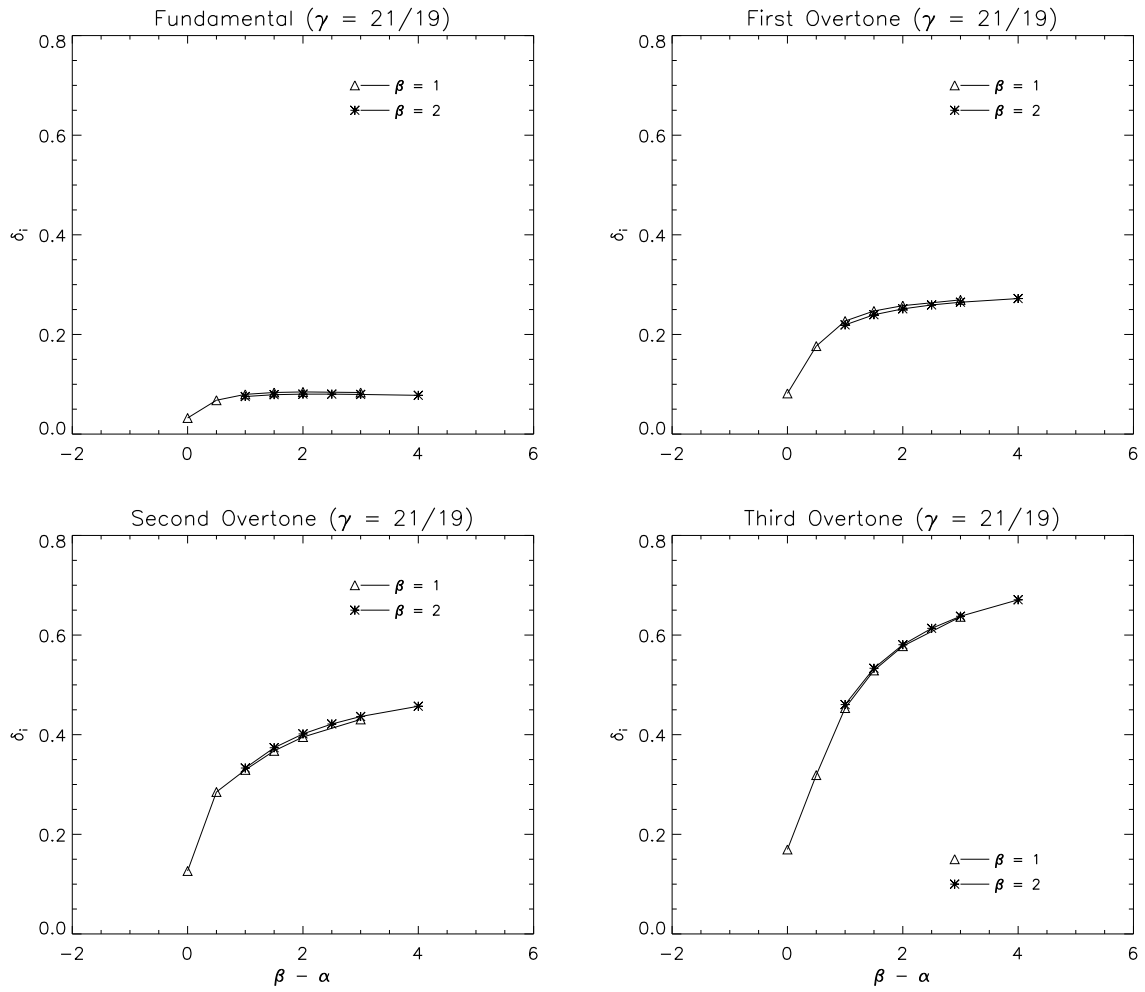


Figure 11. The frequency δ_i is plotted versus $\beta - \alpha$ ($\gamma = 21/19$) for various modes.